

# Extending Qualitative Reconstruction to Biharmonic Scattering with Limited Data

General Ozochiawaeze<sup>1</sup>   Isaac Harris<sup>1</sup>   Peijun Li<sup>2</sup>

<sup>1</sup> Department of Mathematics, Purdue University

<sup>2</sup> Chinese Academy of Sciences

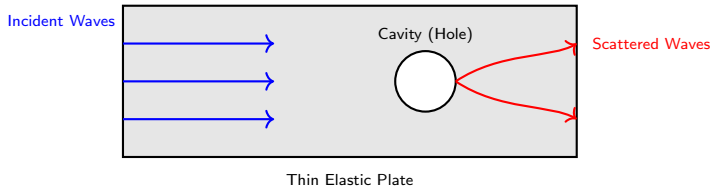
UCI PDE Summer School  
June 2025

# Overview

- 1 Introduction
- 2 Extended Sampling Method (Limited Data)
- 3 Selected Numerical Results

# Physical Intuition: Flexural Waves in Plates

- Send a wave towards an unknown obstacle and measure the reflected wave.
- **Key question:** What can the reflected wave tell us about the obstacle's shape or properties?
- Flexural waves are bending waves traveling in thin elastic plates.
- Modeled by the biharmonic wave equation, which captures plate bending.
- When these waves hit a cavity (hole), they scatter.
- Measuring scattered waves helps identify hidden cavities.



# Applications of Biharmonic Wave Scattering

- **Acoustic Black Hole:**

- Used to control the propagation of sound waves, trapping them within a specific region.

- **Elastic Cloaking:**

- Techniques to make objects undetectable to elastic waves, useful in vibration control.

- **Chladni Plate:**

- The vibrating patterns formed on a plate under the influence of oscillations, representing modal shapes for Electronic Speckle Pattern Interferometry (ESPI).

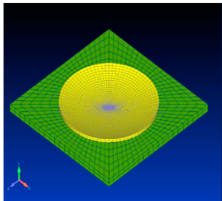


**Figure:** Acoustic Black Hole, American Society of Mechanical Engineers, 2015



**Figure:** Mechanical Cloaking for bridge support design structure

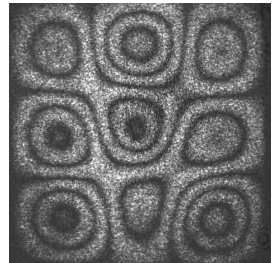


**Figure:** Chladni Plate for ESPI vibration modes

# Biharmonic Clamped Scattering Problem

- Let  $D \subset \mathbb{R}^2$  be a bounded domain such that  $\mathbb{R}^2 \setminus \overline{D}$  is connected.
- The **total field**  $u \in H_{\text{loc}}^2(\mathbb{R}^2 \setminus \overline{D})$  satisfies the **biharmonic wave equation**:

$$\Delta^2 u - \kappa^4 u = 0 \quad \text{in } \mathbb{R}^2 \setminus \overline{D}.$$

- Clamped boundary conditions** on  $\partial D$ :

$$u = 0, \quad \partial_\nu u = 0 \quad \text{on } \partial D,$$

where  $\partial_\nu$  is the outward normal derivative.

- The total field decomposes as

$$u = u^i + u^s,$$

where  $u^i$  is the incident flexural wave and  $u^s$  the scattered wave.

- Incident waves are **time-harmonic plane waves** of the form

$$u^i(x) = e^{i\kappa x \cdot d}, \quad d \in \mathbb{S}^1.$$

- The scattered field  $u^s$  satisfies the biharmonic Sommerfeld radiation condition:

$$\partial_r v - i\kappa v = O(r^{-\frac{3}{2}}) \quad \text{as } r \rightarrow \infty,$$

where  $v = u^s$  or  $\Delta u^s$ .

# Decomposition of the Scattered Field

To analyze the biharmonic scattered field  $u^s$ , we introduce two auxiliary components that separate  $u^s$  into parts satisfying simpler equations:

$$\begin{aligned} u_H^s &:= -\frac{1}{2\kappa^2} (\Delta u^s - \kappa^2 u^s), \\ u_M^s &:= \frac{1}{2\kappa^2} (\Delta u^s + \kappa^2 u^s), \end{aligned}$$

where

$$u^s = u_H^s + u_M^s, \quad \Delta u^s = \kappa^2 (u_M^s - u_H^s).$$

Here,  $u_H^s$  is called the **Helmholtz component**, since it satisfies the Helmholtz equation, while  $u_M^s$  is the **modified (anti-Helmholtz) component**, satisfying a modified Helmholtz equation:

$$\begin{cases} \Delta u_H^s + \kappa^2 u_H^s = 0, \\ \Delta u_M^s - \kappa^2 u_M^s = 0, \end{cases} \quad \text{in } \mathbb{R}^2 \setminus \overline{D}.$$

This decomposition allows us to study  $u^s$  via two second-order PDEs instead of a single fourth-order equation.

# Coupled Scattering Problem

The original biharmonic scattering problem can be reformulated as a coupled system for the Helmholtz and modified Helmholtz components:

$$\begin{cases} \Delta u_H^s + \kappa^2 u_H^s = 0, \\ \Delta u_M^s - \kappa^2 u_M^s = 0, \end{cases} \quad \text{in } \mathbb{R}^2 \setminus \overline{D},$$

with coupled boundary conditions on  $\partial D$ :

$$u_H^s + u_M^s = -u^i, \quad \partial_\nu u_H^s + \partial_\nu u_M^s = -\partial_\nu u^i,$$

and radiation conditions as  $r = |x| \rightarrow \infty$ :

$$\lim_{r \rightarrow \infty} \sqrt{r} (\partial_r u_H^s - i\kappa u_H^s) = 0, \quad \lim_{r \rightarrow \infty} \sqrt{r} (\partial_r u_M^s - i\kappa u_M^s) = 0.$$

**Asymptotic behavior:**

$$|u_H^s| = \mathcal{O}\left(\frac{1}{\sqrt{r}}\right), \quad |u_M^s| = \mathcal{O}\left(\frac{e^{-\kappa r}}{\sqrt{r}}\right),$$

which follows from their Fourier-Hankel expansions and Bessel function asymptotics.

# Coupled Scattering Problem

The original biharmonic scattering problem can be reformulated as a coupled system for the Helmholtz and modified Helmholtz components:

$$\begin{cases} \Delta u_H^s + \kappa^2 u_H^s = 0, \\ \Delta u_M^s - \kappa^2 u_M^s = 0, \end{cases} \quad \text{in } \mathbb{R}^2 \setminus \overline{D},$$

with coupled boundary conditions on  $\partial D$ :

$$u_H^s + u_M^s = -u^i, \quad \partial_\nu u_H^s + \partial_\nu u_M^s = -\partial_\nu u^i,$$

and radiation conditions as  $r = |x| \rightarrow \infty$ :

$$\lim_{r \rightarrow \infty} \sqrt{r} (\partial_r u_H^s - i\kappa u_H^s) = 0, \quad \lim_{r \rightarrow \infty} \sqrt{r} (\partial_r u_M^s - i\kappa u_M^s) = 0.$$

**Asymptotic behavior:**

$$|u_H^s| = \mathcal{O}\left(\frac{1}{\sqrt{r}}\right), \quad |u_M^s| = \mathcal{O}\left(\frac{e^{-\kappa r}}{\sqrt{r}}\right),$$

which follows from their Fourier-Hankel expansions and Bessel function asymptotics.

**Key advantage:** The anti-Helmholtz component  $u_M^s$  decays *exponentially* at infinity, which greatly simplifies analysis and numerical treatment!



# Fundamental Solution and Green's Representation

## Fundamental Solutions of Helmholtz-type Equations

Let  $\Phi_\kappa(x)$  and  $\Phi_{i\kappa}(x)$  be the fundamental solutions in  $\mathbb{R}^2$  of:

$$(\Delta + \kappa^2)\Phi_\kappa(x) = -\delta(x), \quad (\Delta - \kappa^2)\Phi_{i\kappa}(x) = -\delta(x)$$

## Then: Fundamental Solution of Biharmonic Wave Operator

$$G_\kappa(x) = \frac{1}{2\kappa^2} (\Phi_{i\kappa}(x) - \Phi_\kappa(x)), \quad (\Delta^2 - \kappa^4)G_\kappa(x) = -\delta(x)$$

## Green's Representation Formulas

For  $x \in \mathbb{R}^2 \setminus \overline{D}$ , we have

$$u_H^s(x) = \int_{\partial D} [\partial_\nu u_H^s(y) \Phi_\kappa(x-y) - u_H^s(y) \partial_\nu \Phi_\kappa(x-y)] ds(y)$$

$$u_M^s(x) = \int_{\partial D} [\partial_\nu u_M^s(y) \Phi_{i\kappa}(x-y) - u_M^s(y) \partial_\nu \Phi_{i\kappa}(x-y)] ds(y)$$

**Note:** The fundamental solution for the 2D (anti-) Helmholtz equation is given by

$$\Phi_\kappa(x) = \frac{i}{4} H_0^{(1)}(\kappa|x|), \quad \Phi_{i\kappa}(x) = \frac{i}{4} H_0^{(1)}(i\kappa|x|),$$

where  $H_0^{(1)}$  is the Hankel function of the first kind of order zero.

# Far-Field Behavior and the Inverse Problem (Biharmonic)

We recall the fundamental solution of the 2D biharmonic wave operator:

$$G_\kappa(x - y) = \frac{1}{2\kappa^2} [\Phi_{i\kappa}(x - y) - \Phi_\kappa(x - y)]$$

**Far-Field Expansion:**

$$\Phi_\kappa(x - y) = \frac{i}{4} H_0^{(1)}(\kappa|x - y|) \sim \frac{e^{i\kappa|x|}}{\sqrt{|x|}} e^{-i\kappa\hat{x}\cdot y}, \quad \text{as } |x| \rightarrow \infty$$

**Hence,**

$$G_\kappa(x - y) \sim -\frac{1}{2\kappa^2} \cdot \frac{e^{i\kappa|x|}}{\sqrt{|x|}} e^{-i\kappa\hat{x}\cdot y} \quad \text{since } \Phi_{i\kappa} \text{ decays exponentially.}$$

Substituting into Green's representation yields the far-field expansion:

$$u^s(x) = \frac{e^{i\kappa|x|}}{\sqrt{|x|}} u^\infty(\hat{x}) + \mathcal{O}(|x|^{-3/2}), \quad \hat{x} = \frac{x}{|x|}$$

**Far-Field Pattern:**

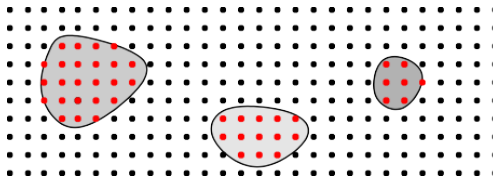
$$u^\infty(\hat{x}) := -\frac{1}{2\kappa^2 \sqrt{8\pi\kappa}} \int_{\partial D} \left[ \partial_\nu u^s(y) e^{-i\kappa\hat{x}\cdot y} - u^s(y) \partial_\nu e^{-i\kappa\hat{x}\cdot y} \right] ds(y)$$

**Inverse Problem:** Given  $u^\infty(\hat{x})$  for all  $\hat{x}$  for one or more incident waves, reconstruct the unknown cavity  $D \subset \mathbb{R}^2$ .

# Sampling Methods

**Examples of sampling methods.** *Linear Sampling Method* (Colton-Kirsch, 1996), *Factorization Method* (Kirsch 1998), *Probe Method* (Potthast, 2001), *Reciprocity Gap Method* (Colton-Haddar, 2005),...

**Principle:** the idea is to construct an indicator test function  $\mathcal{I}(z)$  that will test whether a sampling point  $z$  is in the interior or exterior of the scatterer (i.e.  $\mathcal{I}(z) \approx 1$  inside scatterer,  $\mathcal{I}(z) \approx 0$  outside scatterer).



- (+) Non-iterative, the computation of  $\mathcal{I}$  does not require a forward solver.
- (-) Requires a large amount of multi-static data (many transmitters-receivers).

# Extended Sampling Method

## Extended Sampling Method for Far-Field Measurement

- **Helmholtz equation:** Applied in various works:
  - Juan Liu, Jiguang Sun (2018) – One-wave data
  - Li, Deng, & Sun (2020) – Bayesian method for limited aperture
  - Fang Zeng (2020) – Interior inverse scattering
  - Sun & Zhang (2023) – Inverse source/multifrequency data
- **Elastic wave equation:** Liu, J., Liu, X., & Sun (2019) – One-wave data

## Why Extended Sampling?

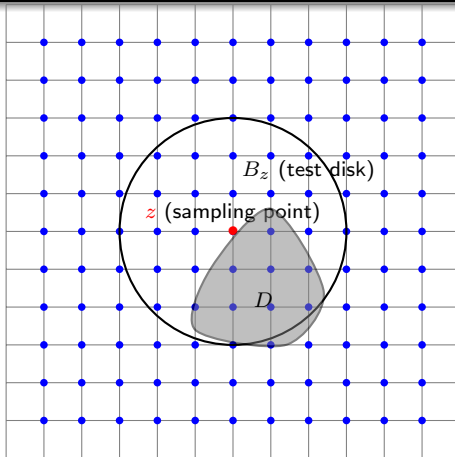
- Versatile: Works with one-wave, multi-wave, and multifrequency data.
- Effective with limited data.

**This talk:** Applying this method to the biharmonic wave equation with one-wave and multifrequency data.

**Key Equation:** The indicator function  $\mathcal{I}(z) := \|g_z\|_{L^2(S^1)}$  comes from solving for the weight function  $g = g_z$ :

$$\underbrace{(\mathcal{F}_{B_z} g)(\hat{x})}_{\text{Superposition of shifted ball's far-field data}} = \underbrace{u^\infty(\hat{x})}_{\text{Measured biharmonic far-field data}} \quad \text{for a single incident angle } d.$$

# Indicator Function Behavior



$\mathcal{I}(z) := \|g_z\|_{L^2(S^1)}$  will take **large** values if  $D \cap B_z = \emptyset$

$\mathcal{I}(z) := \|g_z\|_{L^2(S^1)}$  will take **small** values if  $D \subsetneq B_z$

# Extended Sampling Method: Scattering Problem

Let  $B_z = B(z, R)$  be a sound-soft disk centered at sampling point  $z \in \mathbb{R}^2$ . Define  $U_{B_z}^s(x, \hat{y})$  as the solution of:

$$\begin{cases} \Delta U_{B_z}^s + \kappa^2 U_{B_z}^s = 0 & \text{in } \mathbb{R}^2 \setminus \overline{B_z}, \\ U_{B_z}^s = -e^{i\kappa x \cdot \hat{y}} & \text{on } \partial B_z, \\ \lim_{r \rightarrow \infty} \sqrt{r} (\partial_r U_{B_z}^s - i\kappa U_{B_z}^s) = 0 \end{cases}$$

The far-field pattern  $U_{B_z}^\infty(\hat{x}, \hat{y})$  satisfies:

$$U_{B_z}^\infty(\hat{x}, \hat{y}) = e^{i\kappa z \cdot (\hat{y} - \hat{x})} U_{B_0}^\infty(\hat{x}, \hat{y})$$

**Main Benefit:** Closed-form expression for the far-field pattern of the *unshifted* sound-soft disk  $B_0 = B(0, R)$ :

$$U_{B_0}^\infty(\hat{x}, \hat{y}) = -\frac{e^{-i\pi/4}}{\sqrt{2\pi\kappa}} \left[ J_0(\kappa R) \frac{1}{H_0^{(1)}(\kappa R)} + 2 \sum_{n=1}^{\infty} J_n(\kappa R) \frac{\cos(n\theta)}{H_n^{(1)}(\kappa R)} \right]$$

where  $\theta$  is the angle between  $\hat{x}$  and  $\hat{y}$ .

**Use:** Enables efficient evaluation of  $U_{B_z}^\infty$  via translation.

# Extended Sampling Method Far-Field Equation

Define the operator

$$\mathcal{F}_{B_z} : L^2(\mathbb{S}^1) \rightarrow L^2(\mathbb{S}^1), \quad (\mathcal{F}_{B_z} g_z)(\hat{x}) = \int_{\mathbb{S}^1} U_{B_z}^\infty(\hat{x}, \hat{y}) g_z(\hat{y}) ds(\hat{y}).$$

(ESM Far-Field Equation)

$$\mathcal{F}_{B_z} g_z = u^\infty, \quad \hat{x} \in \mathbb{S}^1$$

**Idea:** For each sampling point  $z$ , solve the above equation for  $g_z$ . If a solution exists, it suggests the unknown cavity  $D \subseteq B_z$ .

**Key Challenge:** This equation is ill-posed since  $\mathcal{F}_{B_z}$  is a compact operator with an analytic kernel.

**Motivation:** This motivates introducing auxiliary operators and regularization techniques to effectively solve the inverse problem.

# Auxiliary Operators and Their Properties

Define two key operators associated with the test disk  $B_z$ :

- $\mathcal{G}_{B_z} : H^{1/2}(\partial B_z) \rightarrow L^2(\mathbb{S}^1)$  maps Dirichlet boundary data  $f$  to the far-field pattern  $V^\infty$  of the radiating solution  $V$  solving

$$\begin{cases} \Delta V + \kappa^2 V = 0, & \text{in } \mathbb{R}^2 \setminus \overline{B_z}, \\ V = f, & \text{on } \partial B_z, \\ \partial_r V - i\kappa V = O(r^{-3/2}), \quad r = |x| \rightarrow \infty. \end{cases}$$

- $\mathcal{H}_{B_z} : L^2(\mathbb{S}^1) \rightarrow H^{1/2}(\partial B_z)$  maps  $g$  to the boundary trace of the Herglotz wave function

$$v_g(x) = \int_{\mathbb{S}^1} g(\hat{y}) e^{i\kappa x \cdot \hat{y}} ds(\hat{y}), \quad x \in \partial B_z.$$

The far-field operator factorizes as

$$\mathcal{F}_{B_z} = \mathcal{G}_{B_z} \circ (-\mathcal{H}_{B_z}).$$

## Key properties:

- If  $\kappa^2$  is not a Dirichlet eigenvalue of  $-\Delta$  on  $B_z$ , then  $\mathcal{H}_{B_z}$  is injective with dense range.
- $\mathcal{G}_{B_z}$  is injective and has dense range.
- Consequently,  $\mathcal{F}_{B_z}$  is injective with dense range.
- All these operators are compact.



# Main Theorem for ESM

## Theorem

Let  $B_z$  be a disk centered at a sampling point  $z$  with radius  $R$ , and let  $D$  be a cavity in a thin plate with clamped boundary conditions. Assume that  $\kappa^2$  is not a Dirichlet eigenvalue of  $-\Delta$  in  $B_z$ . Then, the following hold for the modified far-field equation:

- 1 If  $D \subset B_z$ , then for any  $\epsilon > 0$ , there exists a function  $g_z^\alpha \in L^2(\mathbb{S}^1)$  such that

$$\|\mathcal{F}_{B_z} g_z^\alpha - u^\infty(\hat{x})\|_{L^2(\mathbb{S}^1)} \leq \epsilon. \quad (1)$$

Moreover, the associated Herglotz wave function

$$v_{g_z^\alpha}(x) := \int_{\mathbb{S}^1} e^{i\kappa x \cdot d} g_z^\alpha(d) ds(d), \quad x \in B_z,$$

converges to the solution  $v$  of the Helmholtz equation in  $B_z$  with

$$v = -u_H^s \quad \text{on } \partial B_z$$

as  $\alpha \rightarrow 0$ .

- 2 If  $D \cap B_z = \emptyset$ , then for every  $g_z^\alpha$  satisfying (1) with a given  $\epsilon > 0$ , we have

$$\lim_{\alpha \rightarrow 0} \|g_z^\alpha\|_{L^2(\mathbb{S}^1)} = \infty.$$

# Multilevel Extended Sampling Method (ESM) Algorithm Overview

## 1 Initial Sampling:

- Choose a large radius  $R$ .
- Generate a sampling grid  $T$  with points spaced roughly  $R$  apart.
- Use ESM to find the global minimum point  $z_0 \in T$  of  $\|g_z^\alpha\|_{L^2}$ .
- Set  $D_0$  as an initial approximation of the cavity  $D$ .

## 2 Refinement Loop (for $j = 1, 2, \dots$ ):

- Set finer radius  $R_j = \frac{R}{2^j}$ .
- Generate a finer sampling grid  $T_j$  with points spaced roughly  $R_j$ .
- Find the minimum point  $z_j \in T_j$ .
- If  $z_j \notin D_{j-1}$ , stop and go to Step 3.

## 3 Final Output:

$z_{j-1}$ ,  $D_{j-1}$  as the estimated location and shape of  $D$ .

*This multilevel strategy improves accuracy by zooming in progressively on the cavity location.*

# Numerical Simulation: Multilevel ESM

- **Method:** Multilevel Extended Sampling Method (MESM) used for numerical simulation – multilevel iteratively selects best radius
- **Objective:** Simulate scattering from apple-shaped cavities using varying positions.
- **Subfigures:**
  - **Apple cavity at origin** - Simulation for a cavity centered at the origin.
  - **Apple cavity at (-1.5, 1.5)** - Simulation for a cavity shifted to the position (-1.5, 1.5).
  - **Incident direction**  $d = (1/2, \sqrt{3}/2)$  (fixed).

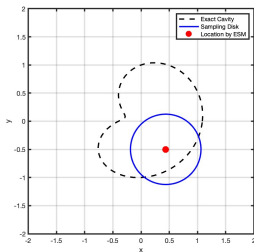


Figure: Apple cavity at origin

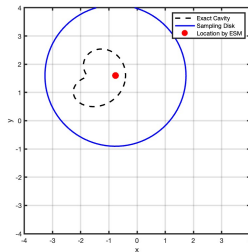


Figure: Apple cavity at (-1.5, 1.5)

# Numerical Simulation: Multilevel ESM

- **Method:** Multilevel Extended Sampling Method (MESM) used for numerical simulation – multilevel iteratively selects best radius
- **Objective:** Simulate scattering from peach-shaped cavities using varying positions.
- **Subfigures:**
  - **Peach cavity at origin** - Simulation for a cavity centered at the origin.
  - **Peach cavity at  $(-1.5, 1.5)$**  - Simulation for a cavity shifted to the position  $(-1.5, 1.5)$ .
  - **Incident direction  $d = (1/2, \sqrt{3}/2)$**  (fixed).

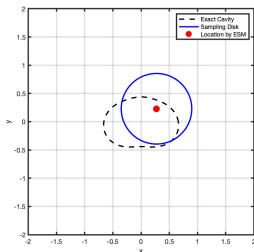


Figure: Peach cavity at origin

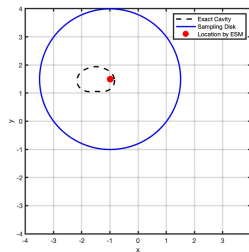


Figure: Peach cavity at  $(-1.5, 1.5)$

# Multi-Incident Direction ESM: Peach Cavity

- **Objective:** Simulate scattering from a peach-shaped cavity at a fixed frequency. Benefit: no need to find best radius  $R$ .
- **Input Data:**
  - $u^\infty(\hat{x}_i, d_j, \kappa)$ : Far-field data for multiple incident directions  $d_j$  at fixed frequency  $2\pi$ .
  - Incident apertures referring to each  $d_j$ :

$$\gamma_2^i = \left\{ (\cos \theta, \sin \theta) \mid \theta \in \left\{ 0, \frac{\pi}{8}, \frac{\pi}{4}, \frac{3\pi}{8}, \frac{\pi}{2} \right\} \right\}$$

$$\gamma_3^i = \left\{ (\cos \theta, \sin \theta) \mid \theta \in \left\{ 0, \frac{\pi}{5}, \frac{2\pi}{5}, \frac{3\pi}{5}, \frac{4\pi}{5}, \pi, \frac{6\pi}{5}, \frac{7\pi}{5}, \frac{8\pi}{5}, \frac{9\pi}{5} \right\} \right\}$$

- Radius  $R = 1$  (fixed)

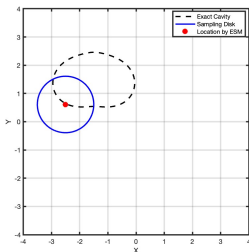


Figure: Peach cavity from  $\gamma_1^i$

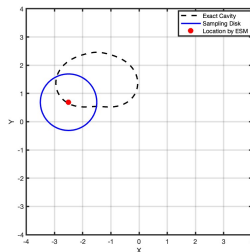


Figure: Peach cavity from  $\gamma_2^i$

# Multifrequency ESM: Peach Cavity

- **Objective:** Simulate scattering from a peach-shaped cavity across multiple frequencies. Benefit: no need to find best radius  $R$
- **Frequency Range:**

$$[\kappa_{\min}, \kappa_{\max}] = \begin{cases} [\pi, 2\pi] & \text{(first frequency range)} \\ [\frac{\pi}{3}, 5\pi] & \text{(second frequency range)} \end{cases}$$

- **Input Data:**

- $u^\infty(\hat{x}_i, d, \kappa_\ell)$ : Far-field data for various incident directions and frequencies.
- Incident direction  $d = (1/2, \sqrt{3}/2)$  (fixed). Radius  $R = 1$  (fixed)
- Frequencies:  $\kappa_\ell$  chosen at 5 distinct frequencies within the specified range.

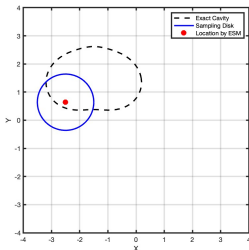


Figure: Peach cavity with range  $[\pi, 2\pi]$

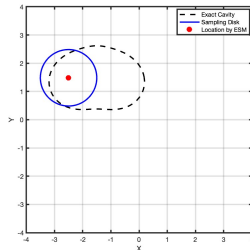


Figure: Peach cavity with range  $[\frac{\pi}{3}, 5\pi]$

## Related: Linear Sampling Method (LSM)

**Goal:** Determine whether a sampling point  $z \in \mathbb{R}^2$  lies inside the unknown cavity  $D \subset \mathbb{R}^2$ .

**LSM Equation:**

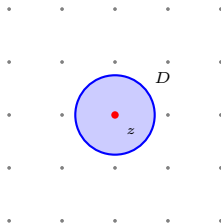
$$\mathcal{F}g_z = G_\kappa^\infty(\cdot, z), \quad (\mathcal{F}g_z)(\hat{x}) := \int_{\mathbb{S}^1} u^\infty(\hat{x}, d) g_z(d) ds(d)$$

Where:

- $\mathcal{F}$ : Far-field operator mapping weights  $g_z$  to superpositions of measured data.
- $G_\kappa^\infty(\cdot, z)$ : Far-field pattern of a biharmonic point source at  $z$ .

**Sampling Principle:**

- *Feasible* (regularized) solutions  $g_z$  exist with small norm if and only if  $z \in D$ .
- *Indicator*: Plotting  $\|g_z\|_{L^2}$  reveals the support of  $D$ . **Same Indicator as ESM!**



# LSM: Recovering the Apple-Shaped Cavity

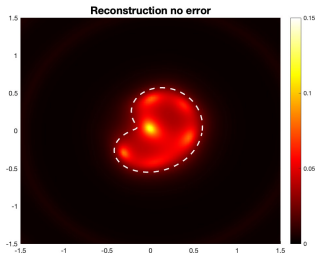


**Figure:** Recovering the Apple-Shaped Cavity with  $\kappa = 2\pi$ ; no noise; 30 incident and observation directions;  $250 \times 250$  grid

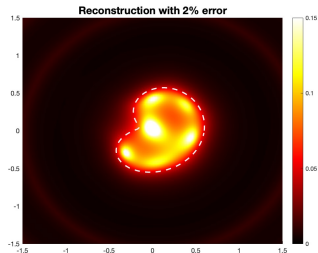


**Figure:** Recovering the Apple-Shaped Cavity with  $\kappa = 2\pi$ ; noise  $\delta = 0.02$ ; 30 incident and observation directions;  $250 \times 250$  grid

**Parametrization of Apple.**  $\gamma(t) = \frac{0.55(1+0.9 \cos t + 0.1 \sin 2t)}{1+0.75 \cos t} (\cos t, \sin t)$



# LSM Result: Recovering the $\partial D \in C^2$ Peach-Shaped Cavity

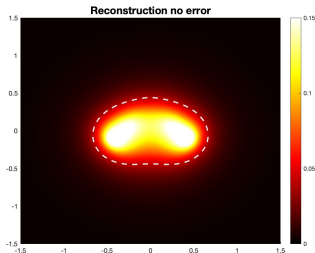


**Figure:** Recovering the Peach-Shaped Cavity with  $\kappa = \pi$ ; no noise; 30 incident and observation directions;  $250 \times 250$  grid

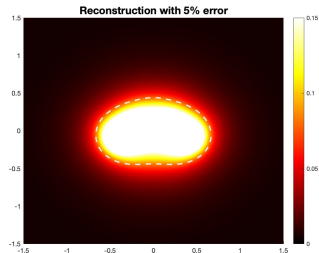


**Figure:** Recovering the Peach-Shaped Cavity with  $\kappa = \pi$ ; noise  $\delta = 0.05$ ; 30 incident and observation directions;  $250 \times 250$  grid

**Parametrization of Peach.**  $\gamma(t) = 0.22(\cos^2 t \sqrt{1 - \sin t} + 2)(\cos t, \sin t)$

# LSM vs. ESM — Key Differences

## Data Requirements:

- LSM requires full multistatic far-field matrix (many incident directions).
- ESM works with limited-aperture or even single-direction data.

## Computation:

- LSM involves solving ill-posed linear systems for each  $z$ .
- ESM reduces to simpler integral equations using known test disks.

**Conclusion:** LSM is classical and reveals more information on scatterer (overall shape and location), but ESM is more practical under data constraints (reveals location only).